Improved FTO/NiO_x Interfaces for Inverted Planar Triple Cation Perovskite Solar Cells

Mohammad Afzaal, Heather M. Yates, Arnaud Walter, and Sylvain Nicolay

***Abstract*—Front electrodes of fluorine doped tin oxide (FTO) thin films and hole transporting layers of nickel oxide thin films have been combined to fabricate 1.063 cm^2 inverted planar solar cells with cesium-containing triple cation perovskites as absorber layers. Using atmospheric pressure chemical vapor deposition FTO layers were obtained with low sheet resistance, decreased root mean square roughness, increased transmission, and reduced optical haze values compared to a widely used commercial FTO substrate. Cell performance outperformed the equivalent cells fabricated using the commercial FTO. With full illumination under maximum power point tracking, a stabilized power conversion efficiency of 13.78 % was obtained for the champion device.**

***Index Terms*—triple cations, perovskite, fluorine doped tin oxide, optical haze, transmission**

I. Introduction

The meteoritic rise in the popularity of single junction perovskite (PK) solar cells is attributed to the strong broadband absorption, long electron-hole diffusion lengths and ambipolar charge transport properties of the organo-halide PK absorber [1]-[3]. These properties along with the availability of low-cost precursors and processing technologies make the PK cell an attractive commercial possibility [4], [5]. Usually, the cells have either planar or infiltrated mesoporous metal oxide structures in a n-i-p or p-i-n solar cell configuration, with the n-i-p reported from suffering from severe hysteresis when measuring the current-voltage characteristic of the devices [6].

For mesoporous (n-i-p) solar cells, fluorine doped tin oxide (FTO) thin films are conventionally used as front electrodes due to their thermal stability during the sintering of the titania scaffolds (the electron-transporting material), which requires high temperatures of 450-500 °C [7]. Such high temperatures are detrimental to indium tin oxide (ITO) surfaces, so these are preferred in inverted planar devices, i.e. p-i-n cells as this allows removal of the mesoporous structure [8], [9]. However, in a highly competitive photovoltaic market, using expensive and limited indium resources faces a massive challenge in large market deployment.

Looking for cost-effective and competitive transparent conductive oxides (TCOs), we exploited FTO's deposited by atmospheric pressure chemical vapor deposition (APCVD) and a commonly used commercial TCO TEC 7 [10] to construct inverted, p-i-n, planar PK solar cells. TEC 7 itself is produced by a CVD in line process by NSG. Various modifications of chemical and physical deposition process are available, however, APCVD is often preferred because of its ability to yield fast deposition rates, high volume, low operating costs, and improved thin film characteristics. In contrast, all physical vapour deposition techniques must be operated at low pressure, which adds considerable operating costs and complexity. In addition, the deposition rates are very much slower. TEC 7 is mainly chosen for PK solar cells due to is its low sheet resistance (Rs = 7.1 Ω $\square^{-1}$) [10]. For a direct comparison, we deposited APCVD FTOs of similar Rs (7.4 Ω $\square^{-1}$), by directing the film thickness through the number of passes of the substrate under the coating head, but with lower root mean square (*RMS*) roughness, increased transmission *(T)* and low haze (*H*). Instability and/or adverse effects of the organic hole transporting layers (HTLs) in PK solar cells has shifted considerable attention towards the use of metal oxide HTLs [11] – [13]. One promising p-type candidate, nickel oxide (NiO_x) is receiving increasing attention because of its high optical transparency, good chemical stability, wide bandgap (~3.6 eV) and deep valence band that aligns well with that of the PK layers [11], [14], [15]. NiO_x is in fact seen as a viable alternative to replace the commonly used spiro-OMeTAD, which apart from its costliness has a complex multi-stage synthesis and poor temperature stability. We demonstrate inverted planar triple cation PK solar cells with an aperture area of 1.063 cm^2 having a configuration of FTO/NiO/$Cs_{0.05}(MA_{0.17}FA_{0.83})_{0.95}Pb(I_{0.83}Br_{0.17})_3$./$C_{60}$/Cu which resulted in power conversion efficiency (PCE) of up to 13.78%. The triple cation PK was used in preference to the methylammonium cation as it is known to result in stabilized structures and increase thermal and moisture stability under operating conditions [16]. To deposit 20 nm NiO_x HTLs on FTO surfaces, magnetron sputtering was utilized. A spin coating process was used to deposit ≈ 300 nm thick triple cation PK coatings. In addition, a mixed halide, rather than just the

This paragraph of the first footnote will contain the date on which you submitted your paper for review. This work is part of the CHEOPS project, which has received funding from the European Union's Horizon 2020 research and innovation programme under grant agreement No. 653296. We thank G. Parr, Salford Analytical Services for the SEM images. *(Corresponding author: Mohammad Afzaal.)*

M. Afzaal was with the Materials and Physics Research Centre, University of Salford, Manchester, M5 4WT, United Kingdom. He is now with the Math & Natural Science Division, Higher Colleges of Technology, P.O.Box: 7947, Sharjah, United Arab Emirates (email: mafzaal@hct.ac.ae)

H. M. Yates is with the Materials and Physics Research Centre, University of Salford, Manchester, M5 4WT, United Kingdom (e-mail: h.m.yates@salford.ac.uk).

A. Walter and S. Nicolay are with the Centre Suisse d'Electronique et de Microtechnique (CSEM), PV-Center, Jaquet-Droz 1, 2002 Neuchâtel, Switzerland (e-mail: arnaud.walter@csem.ch; sylvain.nicolay@csem.ch).

iodide, was used as this has the potential to produce a wider bandgap perovskite solar absorber with a higher voltage output as there is a less potential loss between the work function of NiO_x and valence band of bromine-contained PK [17]. The resulting devices demonstrate the feasibility of producing excellent quality inverted planar triple cation PK solar cells, which generally have better compatibility to high throughput manufacturing processes, than that of the more traditional n-i-p structure. These devices showed minimal hysteresis between forward and reverse IV scans, along with high efficiencies for cells > $1cm^2$. It is worth pointing out here that higher PCEs are reported for mainly ITO, although with some FTO based inverted planar PK solar cells (see later discussion). However, their small cell sizes typically < 0.1 cm^2 can significantly contribute to the measurement errors [18]. In general, to compare PK solar cells with other competing technologies, efficiencies of cell sizes with a minimum of 1 cm^2 should be recorded.

II. EXPERIMENTAL DETAILS

All the chemicals were purchased from Sigma Aldrich Company Ltd and used as received. 1.1 mm borosilicate glass (Corning Eagle) was cleaned with detergent, water, propan-2-ol and dried in air.

Prior to any growth experiments, the atmospheric-pressure chemical vapour deposition system was purged continuously with nitrogen (N_2) for several hours. Thin films were deposited at 600 ± 5 °C using monobutyltin trichloride (MBTC) and 1M aqueous trifluoroacetic acid (TFAA) solution delivered with a Sn precursor to H_2O molar ratio of 1:5. MBTC was vaporised at 123 °C (0.6 L min^{-1} carrier gas) and aqueous TFAA solution was flash evaporated (0.7 L min^{-1} carrier gas). N_2 diluted with 15% oxygen (at a total flow of 1.5 L min^{-1}) was used as the carrier gas. A heated susceptor was translated under the static CVD head in an extracted, open atmosphere, enclosure allowing film growth over 10 × 10 cm (± 2 %) area. The number of passes was fixed at 8 to give multiple samples of the same sheet resistivity and thickness.

X-ray diffraction measurements were performed on a Bruker D8 using a Cu Kα source. Scanning electron microscope images were recorded on a Quanta 250 ESEM. The surface roughness was analysed by atomic force microscopy (NanoScope IIIa, Digital Inst. Ltd., Santa Barbara, California, USA) over a 5 × 5 μm area. Prior to thickness measurements, samples were part etched using zinc powder and hydrochloric acid to form a well-defined step edge. A Dektak 3ST surface profilometer was used to measure film thickness at various points of the samples. Hall effect measurements were performed to determine the carrier concentration and the electron mobility with a lab-built system using an electromagnetic with a pole separation of 10 mm and current of 1 A to give a magnetic flux density of 0.66 T. A lab-built spectrometer consisting of a 75 W xenon lamp and four broadband filters centering on four wavelengths (450, 531, 650, 800 nm) was used to measure haze properties. Transmission and reflection properties were measured on a spectrophotometer (nkd8000, Aquila Instruments Ltd,) between 350 nm and 1100 nm at an incident angle of 30° using s polarisation.

The as-deposited FTO layers were cleaned in a professional glass cleaning machine (Miele) using alkaline and acidic solutions. The NiO_x deposition was carried out in a PVD ClusterTool from Evatec from a NiO_x target. The deposition chamber was evacuated to ~5e-7mbar, and the substrate stage was kept at 60°C throughout the deposition. The sputtering process was conducted under a 150sccm flux of Ar, at a pressure of ~7e-3mbar. The RF power on the target is 150W. The substrates were subsequently annealed in air at 300°C.

After annealing the substrates were transferred to a glovebox under a N_2 atmosphere for spin coating of the perovskite solution.

Two 1.5M stock solutions of PbI_2 and $PbBr_2$ in DMF/DMSO (4:1 vol.:vol.) were prepared. From these solutions, intermediate solutions of $FAPbI_3$ and $MAPbBr_3$ (1.22M) were made. Finally, both solutions were mixed in 5:1 ($FAPbI_3$:$MAPbBr_3$) volume ratio and 5% vol. of CsI from a 1.5M solution in DMSO were added. The spin coating of the solution was made in two steps: first 1000rpm for 10s, second at 6000rpm for 18s. Chlorobenzene was used as the antisolvent and dripped on the spinning substrate 5s before the end of the second step. Substrates were then annealed inside the glovebox at 100°C for 1h.

After annealing substrates were transferred to a thermal evaporation chamber where 20 nm of C60 was evaporated as the ETL followed by the Ag contact.

The cells were characterized under a two-lamp class AAA WACOM sun simulator with an AM1.5g irradiance spectrum at 1000 W/m^2. A cell area of 1.063 cm^2 was defined using a metal mask. The I-V characteristics of the cells were determined under both reverse (from V_{OC} to J_{SC}) and forward (from J_{SC} to V_{OC}) bias. External Quantum Efficiency spectra were acquired on a custom-made spectral response setup equipped with a xenon lamp, a grating monochromator and lock-in amplifiers.

III. RESULTS

Thin films of FTOs were deposited by thermal APCVD at 600 ± 5 °C using vaporized monobutyl tin trichloride (as a tin precursor at 123 °C), flash evaporated 1M aqueous solution of trifluoroacetic acid (as a fluorine dopant source) and nitrogen as a carrier gas, with 15% oxygen gas. Deposited films showed good adhesion to the borosilicate glass and cannot be easily scratched. X-ray powder diffraction patterns of the films (Fig. 1) confirmed the cassiterite phase with a tetragonal structure (JCPDS No: 021-1250). No impurities such as Sn or SnO were detected by XRD in the deposited FTOs, suggesting fully oxidized surfaces. One obvious difference between the commercial TEC 7 and our FTOs is the APCVD increased preferred orientation. It has previously been reported that favorable electrical properties are obtained in polycrystalline FTOs films that exhibit a desired preferred orientation along the (200) plane parallel to the substrate surface [19]. The observed (200) preferred growth can be linked to high film growth rates due to high precursor concentrations [20] (Sn/H_2O ratio 1:5 in the present work), low atomic density and favourable minimum interfacial energy [21], and suppression of flat {101} and {110}

faces in the presence of high halogen-rich gases [22] such as hydrogen fluoride, a by-product of the initial precursors.

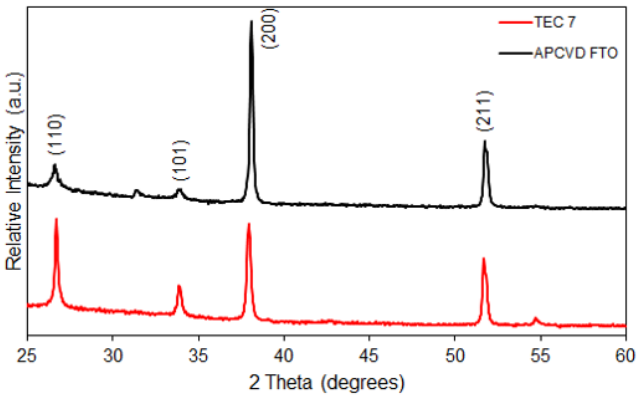

Fig. 1. XRD patterns of FTOs.

The morphological properties of TCOs contribute significantly towards how effectively the excitons are generated. For example, extensively used TEC 7 has a highly textured surface morphology largely composed of pyramidal crystallites with a RMS of ~ 35 nm (Figs. 2a and c) which is ideal for scattering light at the interface and increasing the optical path length of the incident light. As silicon (Si) has poor light absorption properties, this highly rough surface (further discussed below) is ideal for Si-based solar cells [23]. Now the important factor is to maximize the light reaching the absorber layer (without compromising optical and electrical characteristics) to increase the number of electron and hole pairs being produced. A smoother TCO surface scatters less light, so less incident light losses and hence more should be available for transmission. For APCVD FTOs, the morphology is notable different to that of TEC 7 as the films are composed of smaller aggregates (Fig. 2d) and the resulting AFM images (Fig. 2b) showed a smoother surface (RMS ~ 26 nm).

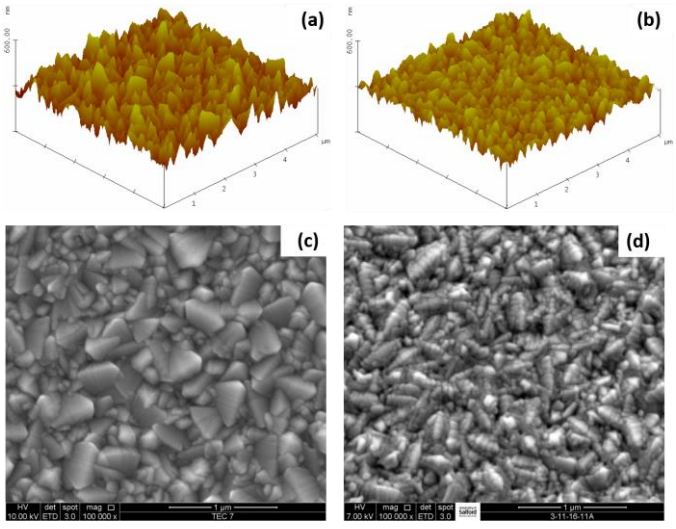

Fig. 2. Images of TEC 7 (a, c) and APCVD FTOs (b, d).

The smooth surfaces of the APCVD deposited FTOs is further corroborated by the haze measurements where the scattering values vary between 0.4 – 8.6 % (wavelength dependent). In contrast, the rougher TEC7 surfaces gave much higher haze values over the same wavelength range of between 2.2 – 14.3 % (Fig. 3). Another important parameter of TCOs is their transmission (*T*) where the deposited FTOs yield excellent *T* values, averaging ~ 83 % between 350 – 1100 nm. For TEC 7, the average decreases to 76 % in the same wavelength range. It is also worth mentioning that due to the geometry of our instrument, *T* and reflection (*R*) measurements are carried out at 30°, not 90° which will marginally reduce *T* and increase *R*. The APCVD FTOs are thicker than TEC 7 (716 ± 28 nm *vs* 600 ± 16 nm), which leads to more prominent interference oscillations for both *T* and *R* spectra. TEC 7 contains an additional thin silica barrier layer between the substrate and FTO thin film [24]. This too modifies and broadens the *T* and *R* spectra for TEC 7.

The APCVD FTOs optical and morphological properties are more suited for use in PK solar cells than the reference FTO. Interestingly, carrier concentrations (*N*) for APCVD FTOs are marginally lower than TEC 7 ($N = 4.0 \times 10^{20}$ cm^{-3} *vs*. 4.8×10^{20} cm^{-3}), which is often needed because of a resulting decrease in free carrier absorption. Our APCVD FTOs are found to be more resistive than TEC 7 (5.30×10^{-4} Ω cm *vs*. 4.25×10^{-4} Ω cm). The improvement in *T* is helped by the lower carrier concentration and reduction in optical scatter. As far as the mobility is concerned, APCVD FTOs have a similar value (29 cm^2/Vs) to that of TEC 7 (31 cm^2/Vs).

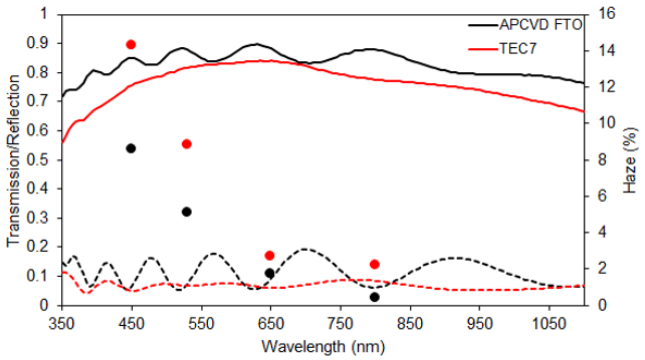

Fig. 3. Optical characteristics of FTOs.

Sputtered NiO_x was used as the HTL due to its reported stability, high optical transparency and ability to provide a much-reduced cell current-voltage hysteresis. Due to this, although the main thrust of the paper is the importance of the FTO properties and how they impinge on the performance of the cells, this section covers some NiO_x characterisation. Samples of NiO_x sputtered directly on glass, on TEC7 and our APCVD FTO were characterised and compared.

Deposition directly on glass established polycrystalline cubic NiO (JCPDS-47-1049) with diffraction signals at 37.0° (111) and 43.3° (200). The signal is relatively weak due to the thinness of the film (20 nm). There was no obvious change in crystallinity when sputtered onto FTO with the NiO (200) peak and (111) as a shoulder on the FTO (200) peak (Fig.4).

The AFM (not given here) and SEM established the very smooth nature of the NiO_x when deposited directly on glass with a mean roughness of approximately 1 nm. When deposited on the FTO the surfaces looked very similar to the original FTO surfaces, with only marginally lower roughness values,

suggesting the NiO_x was deposited conformally. The RMS values for TEC 7

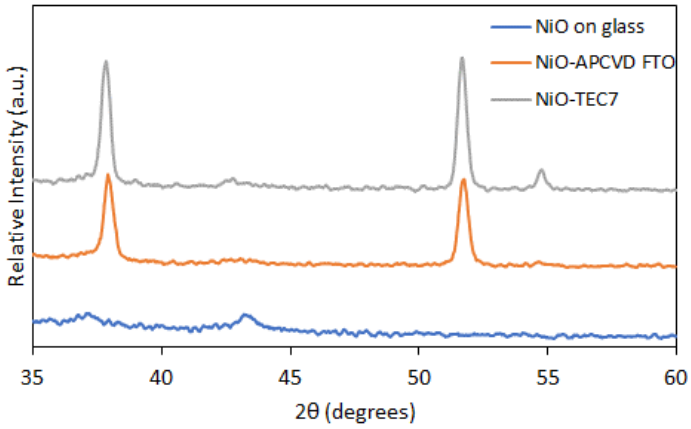

Fig. 4. XRD patterns for sputtered NiO on glass and FTOs.

dropped from 35 nm to 32 nm on NiO_x coating and that of the APCVD FTO showed no change (18 nm).

The presence of the Ni and O was determined by EDAX. The SEM and AFM for the NiO_x/APCVD sample came from a masked FTO sample so only selected areas of the film were coated with NiO_x. The images and EDAX were taken at both positions where NiO_x had been deposited and in between. The lack of morphology changes on addition of the NiO_x confirmed the conformal nature of the coating.

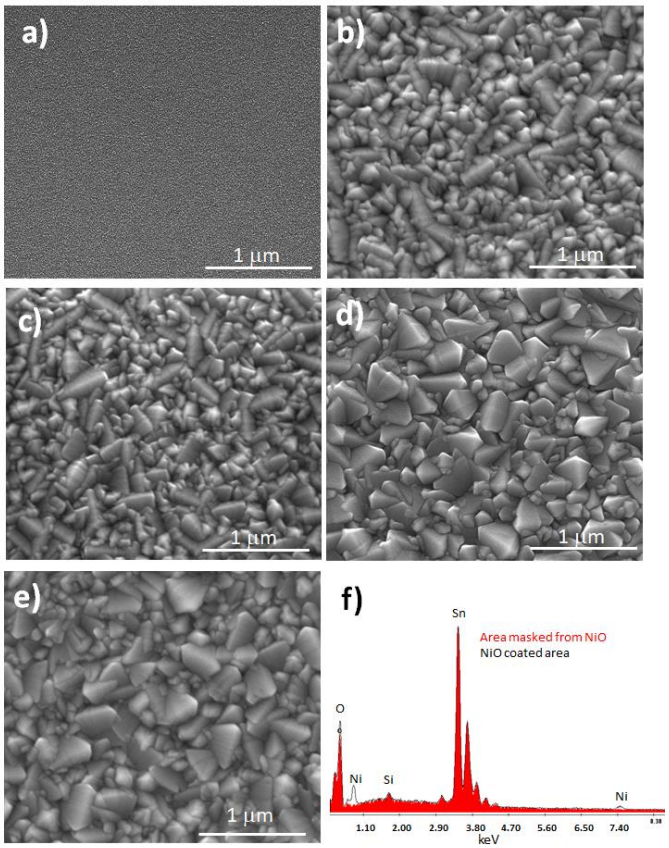

Fig. 5. SEM images of a) NiO on glass, b) NiO_x/APCVD FTO, c) masked area on NiO/FTO film (i.e. no NiO_x), d) NiO_x/TEC7, e) TEC7 and f) EDAX of two areas on patterned APCVD FTO/NiO_x sample.

Optical measurements confirmed the highly transparent nature of NiO_x with an increase in transmission on annealing (Fig. 6a) from 84 to 87% which is most likely to be a result of fewer grain boundaries and consequently reduced optical scattering. In addition, there was no apparent change in the average transmission (350 – 1100 nm) for either type of FTO on addition of the NiO_x coating. Ellipsometry was used to extract the wavelength dependent refractive index (2.0 at 500 nm) and absorption coefficients (Fig. 6b), which is in good agreement to those in the literature [25].

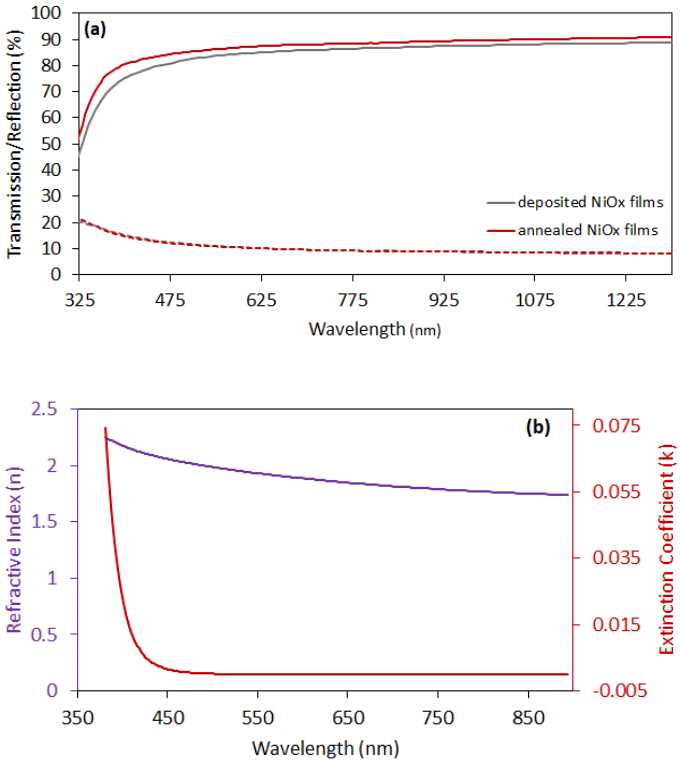

Fig. 6. a) Optical properties of NiO_x on glass (0.5 mm) before and after annealing. b) n and k for sputtered NiO on glass.

Due to the thinness of the NiO coating the sheet resistance for both types of FTO samples with the NiO coating showed no change, within experimental error, to that of the original FTO samples, while an equivalent NiO coating directly on glass was highly resistive.

APCVD FTOs with low *Rs*, *RMS*, *H*, but with high *T* were used to fabricate inverted planar triple cation PK solar cells and their resulting solar cell properties compared with TEC 7. We anticipate that having smooth surfaces should aid the deposition of smooth HTL and PK layers, allowing maximum contact between the layers and efficient charge transfer. As clearly evident in Fig. 7, all narrowly grouped cell properties of APCVD FTOs based cells indicates consistency and reproducibility. Moreover, increased efficiency in cell performance from APCVD FTOs is a combination of the V_{oc}, J_{sc} and FF cell parameters. The gained J_{sc} values, as measured from the IV curves may be a result of increased light harvesting properties of APCVD FTOs. However, the current extracted

from the External Quantum Efficiency (EQE) showed a much smaller improvement with an average of 20.29 mA/cm^2 (σ = 0.15 mA/cm^2) and 19.72 mA/cm^2 (σ = 0.35 mA/cm^2) for the APCVD FTO and TEC 7 based cells, respectively. This suggests that there are other facts having a greater impact such as improved charge collection due to maximized contact between the layers on the smoother FTO. However, a plateau of over 80 % EQE (410 nm to 740 nm) suggests high photon-to-electron conversion in the cells (Fig. 8a). Improved FF and reduced series resistance is usually related to reduced pinholes (low recombination processes) and increased charge collection, respectively. This again aided by the smoother surface of the APCVD FTO, which may lead to better interface integrity with subsequent layers and hence improved quality of the perovskite deposition and so a reduction in cell shunts. Similarly, the mean V_1 value for APCVD FTO is significantly higher than that of the TEC 7 derived cells. Current-voltage scans of champion APCVD FTO based device demonstrated PCE of 13.78 % (Fig. 8b). From the external quantum efficiency curve, derived current density of 20.3 mA cm^{-2} is consistent with the measured value under simulated light.

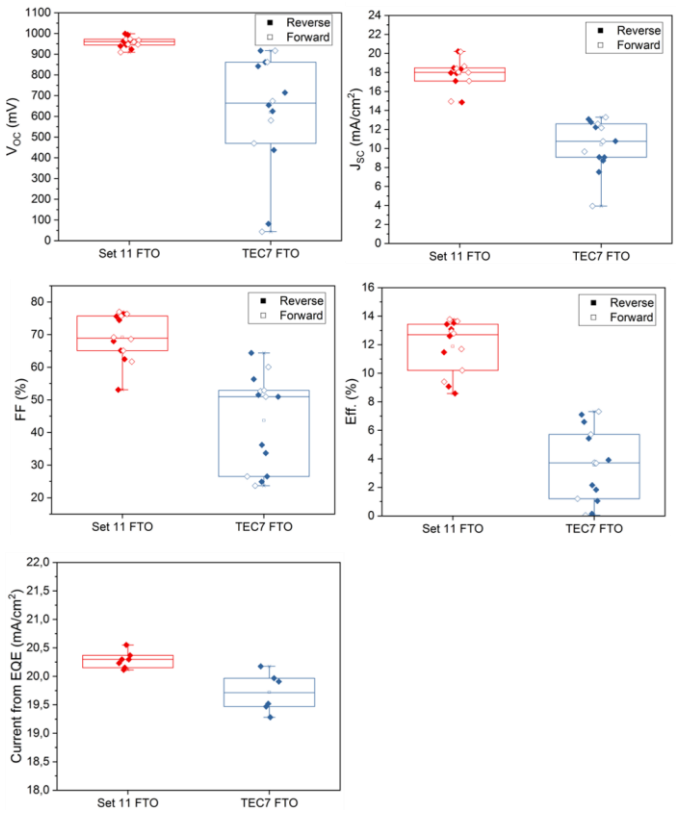

Fig. 7. Statistical box plots of the inverted planar triple cation PK solar cells (note: set 11 FTO labelled on *x* axis denotes APCVD FTO).

Due to the wide variation in p-i-n device composition within the scientific literature, it is very difficult to make direct comparisons between results. Additionally, as previously mentioned, the size of the reported cell can make a large difference in PCE due to the increased likelihood of inclusion of pinholes and/or defects within the area studied [26]. These in turn leading to low resistance shunting paths and a reduction in light absorption. The majority of work on inverted planar cell structures is based on ITO substrates to achieve smooth interfaces. For example, Lai et al. reported a PCE of 7.75 % for ITO/NiO_x/$CH_3NH_3PbI_3$/PCBM/BCP/Al cell structures which involved additional high-temperature annealing at 450 °C [27]. More recently, Weber et al. reported a PCE of 12.8% for a small scale (0.09 cm^2) p-i-n device with a cell configuration of ITO/NiO_x/PK/$PC_{60}BM$/Ag using a $Cs_{0.08}(MA_{0.17}FA_{0.83})_{0.92}Pb(I_{0.83}Br_{0.17})_3$ based PK [28]. This device, although closer to our device material structure is based on an ITO rather than FTO TCO. Other recent work using FTO along with a NiO HTL includes Tang et al [29] who achieved a PCE of 11.82% when using similar thickness NiO to that used by us, with an optimum of 15.47% for a much thicker HTL, albeit with a much smaller cell size of 0.12 cm^2. The authors also emphasized the variation in PCE that is achieved by other researchers dependent on the size, shape, and crystallinity of the NiO. Zhu et al [30] reported PCE of 18.8% for a FTO/NiO/$MAPbI_3$/C60/SnO_2/Ag configuration, is again not directly comparable due to differences in perovskite composition and use of nanocrystallite SnO_2 as the ETL. The effect on cell performance of differing NiO_x, perovskite and PCBM thicknesses is clearly reported by Yin et al [30] showing a wide range in PCE highly dependent on the various film thicknesses. Both Zhu [30] and Yin [31] reported high PCE's for their optimum FTO/NiO based devices, again not directly comparable due to very different film thicknesses, use of only the methylammonium cation and of greater importance the very small sizes of the cells at 0.06 cm^2 and 0.112 cm^2.

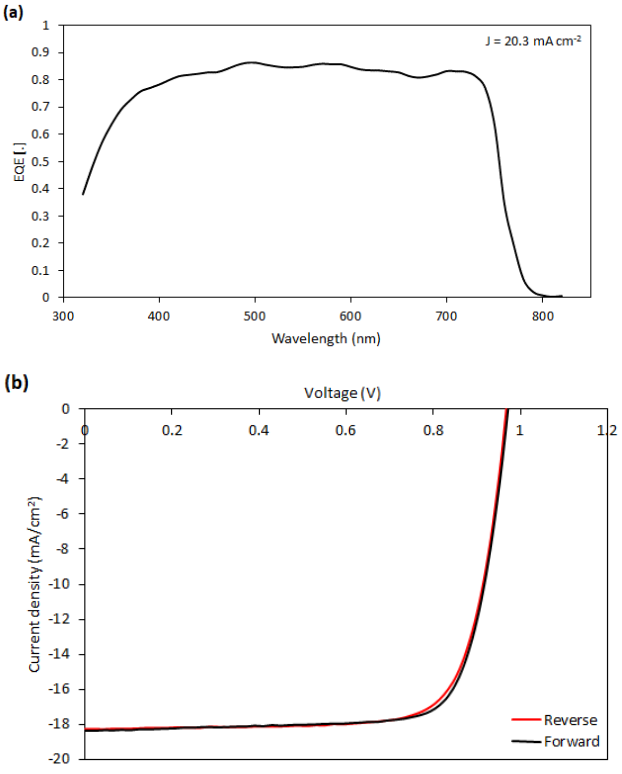

Fig. 8: (a) EQE (b) current-voltage measurements for champion perovskite solar cell.

In addition, the use of NiO_x to enable the formation of a planar p-i-n rather than n-i-p solar cell configuration showed a reduction in hysteresis between the forward and reverse current-voltage characteristics. A comparison between results for planar MALI on our CVD FTO (with TiO_{2-x} ETL) to the present cells showed a factor of 10 reduction in hysteresis as determined from the areas under the forward and reverse IV curves. Hysteresis has been ascribed to the perovskite crystallinity, degree of interface contact [32], excess mobile ionic species and interfacial charge traps [33]. Previous research suggested that perovskite quality is strongly influenced by the underlying substrate [34] so possibly deposition on NiO_x rather than a TiO_{2-x} surface, along with changes to the chemical structure may have improved the crystallinity and interface contact leading to a reduction in interfacial charge traps. Although, a much bigger factor on the cell parameters is the change from the use of NiO_x as the HTL to TiO_{2-x} as an ETL.

IV. Conclusion

We have successfully demonstrated that APCVD deposited FTO front electrodes in conjunction with sputtered NiO_x HTL could be effectively used to construct competitive large area inverted planar triple cation PK solar cells. Unlike commonly used FTO surfaces, smooth FTOs not only aids with improved physical contact between the layers, but also reduces light scattering effects at the surface. The outcome is evident in the form of improved FF/lower series resistance pointing towards reduced pinhole/reduced alternative recombinations.

References

[1] M. M. Lee, J. Teuscher, T. Miyasaka, T. N. Murakami, and H. J. Snaith, "Efficient Hybrid Solar Cells Based on Meso-Superstructured Organometal Halide Perovskites" *Science*, vol. 338, pp. 643-647, 2012, doi: 10.1126/science.1228604.

[2] M. Liu, M. B. Johnston, and H. J. Snaith, "Efficient Planar Heterojunction Perovskite Solar Cells by Vapour Deposition" *Nature*, vol. 501, pp. 395-398, 2013, doi: 10.1038/nature12509.

[3] N. J. Jeon, J. H. Noh, Y. C. Kim, W. S. Yang, S. Ryu, and S. I. Seok, "Compositional Engineering of Perovskite Materials for High-Performance Solar Cells" *Nature*, vol. 517, pp. 476-480, 2015, doi: 10.1038/nature14133.

[4] G. Xing, N. Mathews, S. Sun, S. S. Lim, Y. M. Lam, M. Grätzel, S. Mhaisalkar, and T. C. Sum, "Long-range Balanced Electron-and Hole-Transport Lengths in Organic-Inorganic $CH_3NH_3PbI_3$" *Science*, vol. 342, pp. 344-347, 2013, doi: 10.1126/science.1243167.

[5] Q. Dong, Y. Fang, Y. Shao. P. Mulligan, J. Qiu, L. Cao, and J. Huang, "Electron-Hole Diffusion Lengths > 175 μm in Solution-Grown $CH_3NH_3PbI_3$ Single Crystals" *Science*, vol. 347, pp. 967-970, 2015, doi: 10.1126/science.aaa5760.

[6] (a) J. H. Heo, H. J. Han, D. Kim, T. K. Ahn, and S. H. Im, "Hysteresis-less Inverted $CH_3NH_3PbI_3$ Planar Perovskite Hybrid Solar Cells with 18.1% Power Conversion Efficiency" *Energy Environ. Sci.* vol. 8 pp. 1602-1608, 2015, doi: 10.1039/C5EE00120J. (b) J. Seo, S. Park, Y. C. Kim, N. J. Jeon, J. H. Noh, S. C. Yoon, and S. I. Seok, "Benefits of Very Thin PCBM and LiFL for Solution-Processed p–i–n Perovskite Solar Cells" *Energy Environ. Sci.* vol. 7, pp. 2642-2646, 2014, doi: 10.1039/C4EE01216J. (c) N. J. Jeon, J. H. Noh, Y. C. Kim, W. S. Yang, S. Ryu, and S. I. Seok, "Solvent Engineering for High-Performance Inorganic–Organic Hybrid Perovskite Solar Cells" *Nature Mater*. vol. 13, pp. 897-903, 2014, doi: 10.1038/nmat4014.

[7] W. S. Yang, J. H. Noh, N. J. Jeon, Y. C. Kim, S. Ryu, J. Seo, and S. I. Seok, "High-Performance Photovoltaic Perovskite Layers Fabricated through Intramolecular Exchange" *Science*, vol. 348, pp. 1234−1237. 2015, doi: 10.1126/science.aaa9272.

[8] P. S. C. Schulze, A. J. Bett, K. Winkler, A. Hinsch, S. Lee, S. Mastroianni, L. E. Mundt, M. Mundus, U. Würfel, S. W. Glunz, M. Hermle, and J. C. Goldschmidt, "Novel Low-Temperature Process for Perovskite Solar Cells with a Mesoporous TiO_2 Scaffold" *ACS Appl. Mater. Interfaces* vol. 9, pp. 30567−30574, 2017, doi: 10.1021/acsami.7b05718.

[9] https://www.ossila.com/products/ito-glass-substrate

[10] http://www.mtixtl.com/FTO-252522TEC7-25.aspx

[11] M. B. Islam, M. Yanagida, Y. Shirai, Y. Nabetani and K. Miyano, "NiO_x Hole Transport Layer for Perovskite Solar Cells with Improved Stability and Reproducibility" *ACS Omega* vol. 2, pp. 2291-2299, 2017, doi: 10.1021/acsomega.7b00538.

[12] J. H. Park, J. Seo, S. Park, S. S. Shin, Y. C. Kim, N. J. Jeon, H. W. Shin, T. K. Ahn, J. H. Noh, S. C. Yoon, C. S. Hwang, and S. I. Seok, "Efficient $CH_3NH_3PbI_3$ Perovskite Solar Cells Employing Nanostructured p-Type NiO Electrode Formed by a Pulsed Laser Deposition" *Adv. Mater*. Vol. 27, pp. 4013−4019, 2015, doi: 10.1002/adma.201500523.

[13] A. B. Huang, J. T. Zhu, J. Y. Zheng, Y. Yu, Y.Liu, S. W. Yang, S. H. Bao, L. Lei and P. Jin, "Achieving high-performance planar perovskite solar cells with co-sputtered Co-doping NiO_x hole transport layers by efficient extraction and enhanced mobility" *J. Mater. Chem. C* vol. 4, pp. 10839-10846, 2016, doi: 10.1039/C6TC03624D.

[14] A. Liu, G. Liu, H. Zhu, B. Shin, E. Fortunato, R. Martins and F. Shan, "Hole Mobility Modulation of Solution-Processed Nickel Oxide Thin-Film Transistor Based on High-K Dielectric" *Appl. Phys. Lett*. Vol. 108, pp. 233506, doi: 10.1063/1.4953460.

[15] C. Park, J. Kim, K. Lee, S. K. Oh, H. J. Kang and N. S. Park, "Electronic, Optical and Electrical Properties of Nickel Oxide Thin Films Grown by RF Magnetron Sputtering" *Appl. Sci. Converg. Technol*. Vol. 24, pp. 72-76, 2015, do: 10.5757/ASCT.2015.24.3.72.

[16] M. Saliba, T. Matsui, J.-Y. Seo, K. Domanski, J.-P. Correa-Baena M. K. Nazeeruddin, W. Tress, A. Abate, A. Hagfeldtd and M. Grätzel, "Cesium-containing triple cation perovskite solar cells: improved stability, reproducibility and high efficiency" *Energy Environ. Sci*. vol. 9, pp. 1989-1997, 2016, doi: 10.1039/C5EE03874J.

[17] A. Sahu, and A. Dixit, "Inverted structure perovskite solar cells: A theoretical study" *Curr. Appl. Phys*. vol. 18, pp. 1583-1591, 2018, doi: 10.1016/j.cap.2018.10.008.

[18] W. Chen, Y. Wu, Y. Yue, J. Liu, J. W. Zhang, X. Yang, H. Chen, E. Bi, I. Ashraful, M. Grätzel, and L. Han, "Efficient and Stable Large-Area Perovskite Solar Cells With Inorganic Charge Extraction Layers" *Science* vol. 350. pp. 944-948, 2015, doi: 10.1126/science.aad1015.

[19] M. Soliman, M. M. Hussein, S. El-Atway and M. E. El-Gamal, "Effect of Doping and Spraying Technique on the Properties of Tin Oxide Films" *Renewable Energy* vol. 23, pp. 463–470, 2001, doi: 10.1016/S0960-1481(00)00151-8.

[20] C. Agashe, M. Takwale, V. Bhide, S. Mahamuni, S. K. Kulkarni, "Effect of Sn Incorporation on the Growth Mechanism of Sprayer SnO_2 Films" *J. Appl. Phys*. vol. 70, pp. 7382–7386, 1991, doi: 10.1016/0167-577X(91)90135-S.

[21] A. Smith, J.-M. Laurent, D. S. Smith, J.-P. Bonnet and R. Clemente, "Relation Between Solution Chemistry and morphology of SnO_2-based Thin Films Deposited by a Pyrosol Process" *Thin Solid Films* vol. 266, pp. 20-30, 1995, doi: 10.1016/0040-6090(95)06648-9.

[22] J. T. Wang, X. L. Shi, X. H. Zhong, J. N. Wang, L. Pyrah, K. D. Sanderson, P. M. Ramsey, M. Hirata and K. Tsuri, "Morphology Control of Fluorine-Doped Tin Oxide Thin Films For Enhanced Light Trapping" *Sol. Energy Mater. Sol. Cells* vol. 132, pp. 578-588, 2015, doi: 10.1016/j.solmat.2014.09.043.

[23] H. M. Yates, P. Evans, D. W. Sheel, S. Nicolay, L. Ding, and C. Ballif, "High-Performance Tandem Silicon Solar Cells on F:SnO_2" *Surf. Coat. Technol*. Vol. 230, pp. 228–233, 2013, doi: 10.1016/j.surfcoat.2013.05.029.

[24] A. Mills, N. Elliott, I. P. Parkin, S. A. O'Neill and R. J. Clark, "Novel TiO_2 CVD Films for Semiconductor Photocatalysis" *J. Photochem. PhotoBiol*. A vol. 151, pp. 171-179, 2002, doi: 10.1016/S1010-6030(02)00190-9.

[25] B. Sasi K. G. Gopchandran, P. K. Manoj, P. Koshy, P. P. Rao and V. K. Vaidyan, "Preparation of Transparent and Semiconducting NiO Films"

Vacuum. Vol. 68, pp. 149–154, 2003, doi: https://doi.org/10.1016/S0042-207X(02)00299-3.

[26] J. Werner, C. H. Weng, A. Walter, L. Fesquet, J. P. Seif, S. De Wolf, B. Niesen and C. Ballif, "Efficient Monolithic Perovskite/Silicon Tandem Solar Cell with Cell Area >1 cm^2" *J. Phys. Chem. Lett.* Vol. 7, pp. 161-166, 2016, doi: 10.1021/acs.jpclett.5b02686.

[27] W.-C. Lai, K.-W. Lin, T.-F. Guo and J. Lee, "Perovskite-based solar cells with nickel-oxidized nickel oxide hole transfer layer" *IEEE Trans. Electron Dev*. vol. 62, pp. 1590–1595, 2015, doi: 10.1109/TED.2015.2413671.

[28] S. Weber, T. Rath, J. Mangalam, B. Kunert, A. M. Coclite, M. Bauch, T. Dimopoulos, and G. Trimmel, "Investigation of NiO_x-hole transport layers in triple cation perovskite solar cells" *J. Mater. Sci. Mater. Electron* vol. 29, pp. 1847-1855, 2018, doi: 10.1007/s10854-017-8094-9.

[29] S. Tang, D. Jiao L. Zhang, X. Zhang, C. Xu, C. Yao, J. Wu, Z. Lan, "High-performance inverted planar perovskite solar cells based on efficient hole-transporting layers from well-crystalline NiO nanocrystals" *Solar Energy*, vol. 161, pp.100-108, 2018, doi: 10.1016/j.solener.2017.12.045.

[30] Z. Zhu, Y. Bai, X. Liu, C. C. Chueh, S. Yang and A. K. Jen, "Enhanced efficiency and stability of inverted perovskite solar cells using highly crystalline SnO_2 nanocrystals as the robust electron transporting layer" *Adv. Mater*. vol. 28, pp. 6478-6484, 2016, doi: 10.1002/adma.201600619.

[31] X. Yin, Z. Yao, Q. Luo, X. Dai, Y. Zhou, Y. Zhang, Y. Zhou, S. Luo, J. Li, N. Wang and H. Lin, "High efficiency inverted planar perovskite solar cells with solution-processed NiO_x hole contact" *ACS Appl. Mater. Interf.* vol. 9, pp. 2439−2448, 2017, doi: 10.1021/acsami.6b13372.

[32] E. L. Unger, E. T. Hoke, C. D. Bailie, W. H. Nguyen, A. R. Bowring, T. Heumüller, M. G. Christoforo and M. D. McGehee, "Hysteresis and transient behavior in current-voltage measurements of hybrid perovskite absorber solar cells" *Energy Environ. Sci*. vol. 7, pp. 3690-3698, 2014, doi: 10.1039/C4EE02465F.

[33] Y. Zhang, M. Liu, G. E. Eperon, C. T. Leijtens, D. McMeekin, M. Saliba, W. Zhang, M. de Bastiani, A. Petrozza, L. M. Herz, M. B. Johnston, H. Lin, H. J. Snaith, "Charge selective contacts, mobile ions and anomalous hysteresis in organo-inorganic perovskite solar cells" *Mater. Horiz*. vol. 2, pp. 315-322, 2015, doi: 10.1039/C4MH00238E.

[34] J. You, L. Meng, T. B. Song, T. F. Guo, Y. M. Yang, W. H. Chang, Z. Hong, H. Chen, H. Zhou, Q. Chen, Y. Liu, N. De Marco, and Y. Yang, "Improved air stability of perovskite solar cells via solution processed metal oxide transport layers" *Nat. Nanotechnol*. vol. 11, pp. 75-81, 2016, doi: 10.1038/nnano.2015.230.